

Optically Tunable Properties of Small Organic Molecules via Photomediated Aza Nazarov Cyclizations

Arya K. Rajan,[‡] Pravien S. Rajaram,[‡] Keerthana Chakkanalil, Sayantani Ghosh,^{*} and Ryan D. Baxter^{*}



Cite This: <https://doi.org/10.1021/acs.joc.5c01311>



Read Online

ACCESS |



Metrics & More

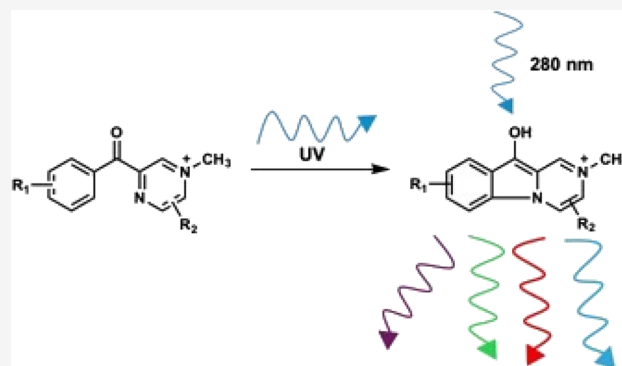


Article Recommendations



Supporting Information

ABSTRACT: We unveil the spectral characteristics exhibited by a group of benzoyl methyl pyrazinium molecules undergoing aza-Nazarov photocyclization to luminescent pyrazino-indoles upon ultraviolet (UV) irradiation between 280 and 400 nm. The reaction, driven by photogenerated radical formation, induces structural transformations that manifest as a striking red-shift of up to 100 nm in the photoluminescent spectra, a highly unusual and visually discernible spectral change. Chemical substitutions further allow fine-tuning of these spectral properties before and after cyclization, offering an additional degree of control over the optical characteristics. Further, when deposited as thin films, the progression of photocyclization can be precisely regulated, enabling the molecules to remain highly fluorescent while arresting the cyclization at desired stages. This ability to modulate the spectral emission by controlling the extent of photocyclization presents unprecedented opportunities for designing advanced functional materials with tailored light-matter interactions for biological and environmental applications. The byproduct-free nature of the reaction, coupled with the tunable optical properties achieved through variations in concentration, solvent, and excitation wavelength, further accentuates the uniqueness of these molecules in the development of materials with customized spectral responses.



INTRODUCTION

Luminescent organic molecules have found numerous applications due to their unique optical properties stemming from their molecular structure and photophysical behavior. Unlike inorganic semiconductors or metal complexes, these organic molecules can be synthetically tailored with precise control over their chemical composition, allowing for the fine-tuning of their optical properties, such as absorption and emission wavelengths, quantum yields, and excited-state lifetimes. It is this unique combination of synthetic versatility, tailorable photophysics, and processing advantages that make luminescent organic molecules attractive for diverse applications spanning optoelectronics, bioimaging, sensing, and energy conversion technologies.^{1–10}

While these molecules offer numerous advantages and applications, they also have some drawbacks and limitations. These include photochemical and thermal instability,¹¹ complex chemical synthesis,^{12,13} toxicity,^{14,15} and difficulty fine-tuning the emission wavelengths.¹⁶ Vulnerability to factors like pH, temperature, or the requirement of specific analytes¹⁷ can also be a drawback when requiring stable and consistent luminescence.¹⁸ More importantly, their spectral properties can differ significantly between solution and solid (thin film) states due to various factors, such as aggregation and intermolecular interactions, leading to shifts or broadening of the emission spectra compared to solution¹⁹ and potential

quenching effects, reducing the overall luminescence efficiency in thin films.²⁰ For organic molecules that undergo photocyclization, there are examples where the reaction is arrested or hindered when they are deposited in a thin film or dispersed in polymer matrices.^{21,22} The solid-state environment can reduce molecular mobility, increase steric constraints, and restrict conformational changes, effectively arresting or suppressing^{23–26} the photochemical transformations that occur readily in solution.

In this paper, we report an efficient, clean, and byproduct-free aza-Nazarov photocyclization reaction that transforms benzoyl methyl pyrazinium salts (R-BMT) to polycyclic pyrazino[1,2-*a*]indoles (R-PIMT) under UV irradiation and ambient conditions. While similar transformations have been proposed previously, we have developed a new synthetic route to well-behaved tetrafluoroborate salts that provide efficient and reproducible photocyclization for several structural analogues.^{27–30} We find both pre- and postcyclization

Received: May 30, 2025

Revised: September 29, 2025

Accepted: October 23, 2025

molecules to be strongly photoluminescent, and the reaction time to be controllably variable from hours to seconds by tuning molecular concentration. We additionally control the time scale by selecting specific excitation wavelengths within the active 280–400 nm spectral range and find that cyclization proceeds rapidly, in less than 60 min, under incident sunlight. Through minor substitutional changes, we demonstrate that this family of salts can be rationally designed by substitution of 'R' to allow tuning their emission over nearly the entire visible spectrum, including R = H, Br, CH₃, and CN. Finally, we confirm that the reaction can be arrested at any chosen point when the molecules are deposited as a thin film.

RESULTS AND DISCUSSION

Figure 1A presents a series of photographs depicting the color change of H-BMT (dissolved in acetonitrile over a 55 min

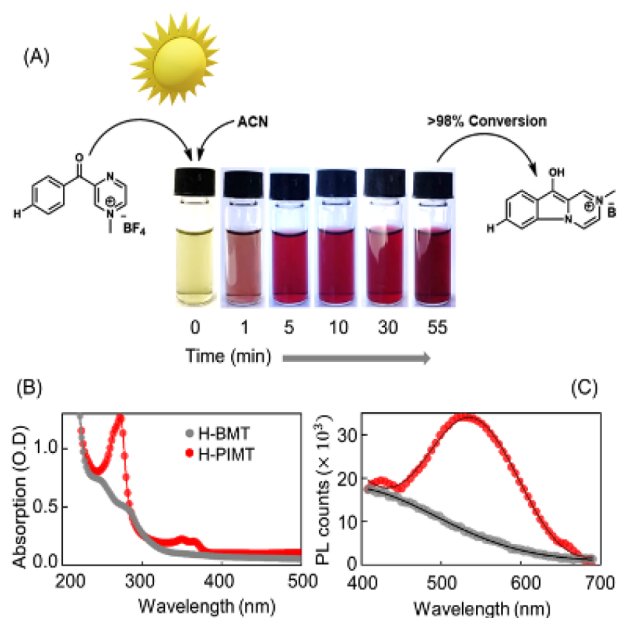


Figure 1. (A) H-BMT in ACN undergoes rapid conversion under ambient sunlight to H-PIMT, accompanied by a visual color change. (B) Absorption and (C) PL emission of H-BMT and H-PIMT, revealing significant differences in their spectral properties, with increased absorption around 360 and 280 nm and emission centered at 530 nm after 100% conversion.

period) resulting from the cyclization process. NMR spectroscopy (Figures S1 and S2 and Table S1) confirms the final product as 98% H-PIMT. The reaction is also efficient using methanol as solvent, and electron paramagnetic resonance spectroscopy (EPR) supports the formation of organic radicals upon irradiation with UV light (Figures S5 and S6). In addition, heterocoupled adducts are observed via high-resolution mass spectrometry (Figure S7) when the reaction is performed in the presence of known organic radical traps. Mass spectrometry and NMR analysis confirm that only H-BMT and H-PIMT are present in solution, with quantitative mass balance confirming the absence of side-products. Figure 1B,C illustrates the UV–vis absorption and photoluminescence (PL) data for the precyclized (H-BMT) and fully cyclized (H-PIMT) species. The absorbance profile for H-PIMT shows increased absorption at 280 nm and in the 350–400 nm range compared to H-BMT. The corresponding PL

emission spectrum, obtained under 280 nm excitation, reveals the emergence of a broad emission peak centered around 530 nm upon complete cyclization. PL quantum yield (PLQY) measured in solution is 17%.

Figure 2A presents a spectrally resolved PL emission map showing the gradual evolution of emission intensity and

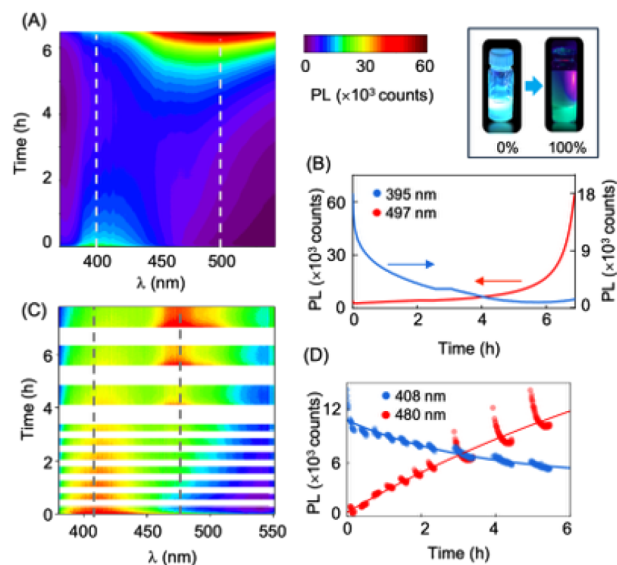


Figure 2. (A) PL emission intensity of H-BMT in ACN plotted as functions of emission wavelength λ and time of exposure to continuous 280 nm excitation. (B) Linecut of (A) plotting the PL intensity at spectral positions denoted by dashed lines on the map as a function of photoexposure time. (C) PL emission of H-BMT in ACN when excitation is interrupted at intervals denoted by the gaps in the map. (D) Same procedure followed for (B). The interruptions allow conversion to H-PIMT to proceed. *Accompanying photo:* Fluorescence images of H-BMT and H-PIMT solutions under UV illumination.

wavelength upon continuous 280 nm excitation, as the cyclization from H-BMT to H-PIMT progresses. The map demonstrates the transition between the initial and final stages, shown in Figure 1C. Figure 2B plots the PL intensity variations over time for the two emission peaks observed in Figure 2A. Initially, the spectrum exhibits an emission peak centered at 395 nm, which gradually diminishes, while a new peak around 497 nm emerges and increases in intensity. Over the 6 h time frame, the 395 nm peak is nearly entirely quenched, and the 497 nm peak grows exponentially in intensity.

Figure 2C shows a similar measurement, but with the 280 nm excitation interrupted at 10 min intervals for the first 3 h, followed by 30 min intervals. The results indicate that the photocyclization reaction is not reversed during the dark periods, either before or after the 3 h mark, and the spectral transformation proceeds almost identically to that in Figure 2A, highlighting the stability of the H-PIMT molecules. Figure 2D further confirms this observation by plotting the PL intensity with an interrupted exposure time. The emissions for both populations proceed almost continuously along the fitted curves despite the interruptions, although the rates of change vary almost linearly with time, in contrast to the exponential change observed under continuous photo exposure.

Chemical substitution is a straightforward approach to modify the properties of BMT molecules.³¹ We employ identical photoexcitation protocols for Br-BMT, CH₃-BMT, and CN-BMT, and we observe results like those of H-BMT.

These substituted molecules undergo photocyclization into their corresponding PIMT counterparts, accompanied by the expected spectral emission changes. The PL peak positions remain approximately in the same ranges as H-BMT/H-PIMT, suggesting that simple substitution is insufficient to induce significant differences (Figure S7), though the PLQY does vary from 10%, 5%, and 8% for Br-PIMT, CH₃-PIMT, and CN-PIMT, respectively. Figure 3A presents a representative

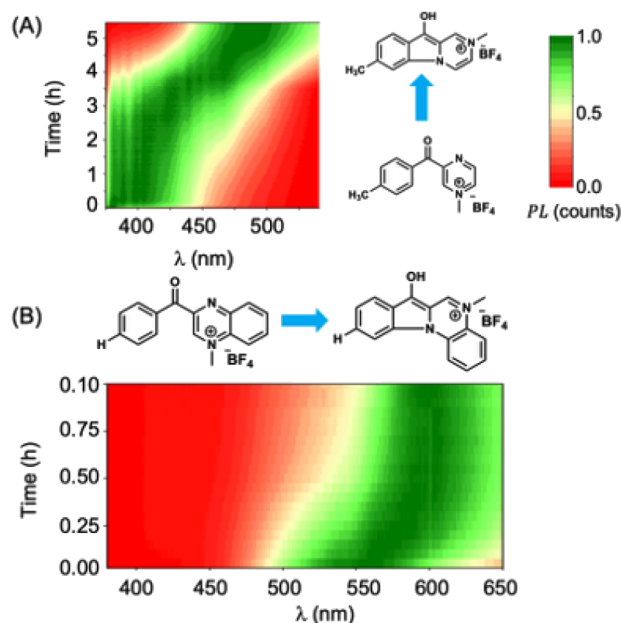


Figure 3. PL emission intensity of (A) CH₃-BMT and (B) Qin-BMT in ACN plotted as functions of emission wavelength λ and time of exposure to continuous 280 nm excitation.

example of the normalized PL emission of CH₃-BMT in CAN under a 280 nm excitation. Initially, the emission peak is centered at ~400 nm, and over the course of 5 h, it shifts to ~480 nm as CH₃-PIMT is formed. Both the time scale and emission changes are comparable to those observed in Figure 2. In contrast, a hierarchical chemical structure with an additional aromatic ring, as shown in Figure 3B, exhibits a more pronounced difference. The extended conjugation leads to increased delocalization of π -electrons,³² resulting in a red-shift of the emission spectrum. Consequently, the precyclized version (Qin-BMT) emits at a longer wavelength, centered at 530 nm. The photocyclization process for Qin-BMT is comparatively rapid, occurring within 10 min, and the resulting Qin-PIMT emits at 610 nm.

While structural modifications are expected to influence photocyclization, they are less interesting, as they cannot be controlled by external factors or performed *in situ*. In Figure 4, we focus on H-BMT and document the variations resulting from changes in the excitation wavelength and concentration. Figure 4A plots the peak wavelength of the PL emission as a function of exposure time for the data in Figure 2A, with 280 nm excitation and H-BMT dissolved in ACN at a concentration of 0.25 mM. Figure 4B presents similar data at a higher concentration (2.0 mM). Notably, the emission of H-BMT itself is red-shifted by nearly 50 nm compared to the 0.25 mM solution, likely due to increased intermolecular interactions causing energy-transfer-related red-shifts at higher concentrations. The emission upon cyclization is shifted from

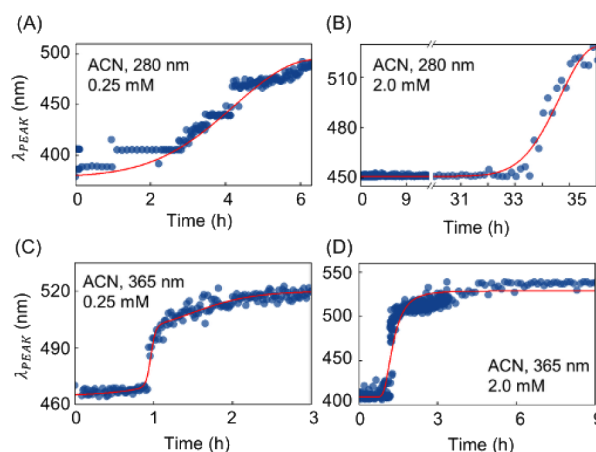


Figure 4. Peak wavelength of PL emission tracked over time for H-BMT in ACN and illuminated with 280 nm excitation at (A) 0.25 and (B) 2.0 mM concentration. H-BMT in ACN illuminated with 365 nm excitation at (C) 0.25 mM and (D) 2.0 mM concentration.

the precyclized value by approximately 90 nm in both cases. However, the most significant difference is in the time scale, with photocyclization being considerably slower in Figure 4B, taking nearly six times longer. Figure 4C,D presents similar measurements with 0.25 and 2.0 mM H-BMT in ACN exposed to 365 nm excitation. This excitation wavelength is selected, as it is where the second most prominent absorption peak is observed in Figure 1B. For a viable comparison between the two excitation wavelengths, the incident power is adjusted to allow for the difference in the absorption efficiency at the different spectral regions (Figure 1B and the Experimental Section). The shift in peak wavelength is noticeably different in both functional form and time scale compared to those in Figure 4A,B. Photocyclization occurs faster for both concentrations under 365 nm excitation, and the transition is less gradual, although the higher concentration still takes longer. The trend of concentration slowing cyclization is further supported by NMR data of the reaction at different light exposure times (Figure S8).

This concentration-dependent behavior can be explained by the absorption spectra in Figure 1B. H-PIMT has higher overall absorbance than H-BMT. Therefore, once both molecular species coexist, H-PIMT prevents photoradicalization of H-BMT by absorbing the incident light itself, hindering the latter's transformation. This effect is magnified as the concentration increases. The reason for 365 nm excitation driving photocyclization with higher efficiency is less clear, though the data show that H-PIMT absorbs far less at this wavelength than at 280 nm, suggesting reduced competition between the two molecular species. The efficacy of excitation at lower wavelengths also explains the faster conversion observed in Figure 1A when H-BMT is exposed to ambient sunlight, which has a higher spectral weight in the region above 360 nm compared to below 300 nm.

Fluorescent materials in liquid form have a wide range of potential uses, such as tracers, labels, or indicators in flow cytometry, environmental monitoring, and even as photosensitizers in photodynamic therapy.^{33–39} These applications leverage the materials' ability to provide real-time, *in situ* information about the presence, concentration, or spatial distribution of specific analytes or biomolecules. However, liquid-based fluorescent materials also have potential limi-

tations and shortcomings that need to be considered. Stability is a key concern, as the fluorescent properties of the molecules may degrade over time due to environmental factors; leaching and contamination risks are also important, potentially leading to unintended consequences or interference with the desired functionality. Scalability is another significant challenge for liquid-based fluorescent materials. Producing and formulating large volumes of stable, consistent fluorescent solutions at a commercial scale can be far more challenging, resource-intensive, and expensive compared with solid or thin film-based fluorescent materials. Recognizing these limitations, our focus shifts toward exploring the potential of these molecules in solid or thin film form. By immobilizing the fluorescent molecules in a solid matrix or depositing them as thin films on substrates, we can potentially address many of the stability, leaching, and scalability issues associated with liquid-based materials.

As mentioned in Section 1, deposition and drying on substrates often lead to quenched PL in luminescent molecules. However, as demonstrated by the image of a free-standing thin film of 100% H-PIMT in poly(vinyl alcohol) (PVA) under UV illumination in Figure 5A, the molecules remain strongly emissive in solid form. PVA offers several advantages as a host polymer, including transparency, water solubility, and ability to form thin films easily. It is nontoxic, biocompatible, and relatively inexpensive. Additionally, PVA's hydroxyl groups can interact with many luminescent molecules, potentially enhancing their stability, and when films are formed from solutions at partial stages of photocyclization, the transformation is arrested upon drying, and the emission is stabilized. Figure 5B presents a series of spatially resolved scanning PL maps depicting the emission intensity over 10 by 10 mm² areas for three films. Each film is fabricated by depositing H-BMT/H-PIMT solutions that have undergone photocyclization to the extent indicated by the percent values, which are determined using NMR. The emission intensity from the films increases with the relative proportion of H-PIMT, with a 3-fold increase observed between 16% and 100% cyclization. The recombination lifetimes of photogenerated charges in the same samples are mapped in Figure 5C over the same areas of the films. Lifetimes decrease with an increased cyclization. Photoluminescence yield is related to the total lifetime (t) extracted through exponential fits to time-resolved PL data and the radiative recombination rate.³⁵ The observed increase in yield coupled with a decreasing total lifetime suggests that the radiative rate decreases with increasing cyclization. This is generally a positive indicator, implying improved luminescence efficiency, enhanced light–matter interaction, and reduced nonradiative losses. Along with a high PL yield, the films exhibit stability over months under ambient conditions, maintaining a uniform and high-intensity emission.

In addition to photocyclization being arrested, emission in thin films is at a lower wavelength. Figure 5D plots the emission wavelengths of the films along with the solution emission of 100% H-BMT and H-PIMT for comparison. The emission wavelengths span a slightly narrower range than in solution, with the film synthesized from 100% H-PIMT solution emitting about 15 nm lower than its solution counterpart. Figure 5E shows that H-BMT adopts a twisted configuration with a 2.9 Å separation between the rings that form the cyclized bond, while H-PIMT has a planar orientation with a reduced separation of 1.3 Å, as revealed by single-crystal

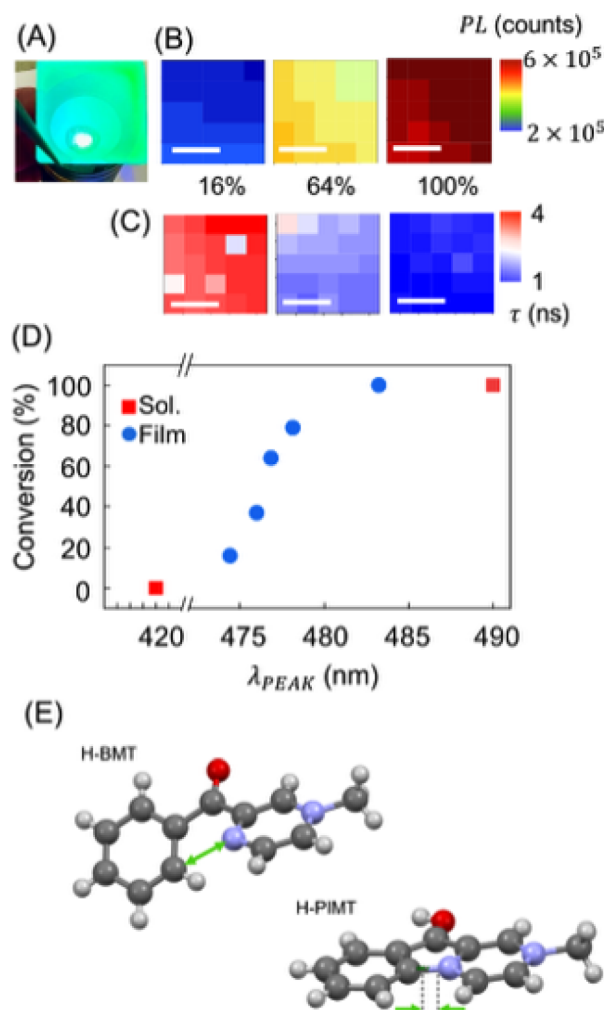


Figure 5. (A) H-PIMT in PVA as a solid film under 280 nm excitation. (B) Spectral emission intensity and (C) recombination lifetimes mapped over 10 by 10 mm² area of films fabricated from H-BMT in solution when 16, 64, and 100% of the molecule has been converted to H-PIMT. Scale bars: 5 mm. (D) Conversion percentage of H-PIMT varying with peak wavelength λ_{PEAK} of spectral emission in both solution and film forms. (E) H-BMT and H-PIMT molecular orientations in the crystalline state, obtained from single-crystal XRD data (Figures S3 and S4). Double-headed arrows indicate the positions and distances where cyclization occurs. Figures are drawn with 50% probability of ellipsoids.

X-ray diffraction.³¹ The twisted structure of H-BMT in the solid state may hinder its ability to transform into planar H-PIMT. Moreover, the planar structure of H-PIMT enables the formation of H-aggregates in the solid state, where molecules pack closely and parallel to each other. This arrangement leads to higher energy excited states in the solid ensemble, resulting in a blue-shift of the emission spectra compared to isolated molecules.⁴⁰

CONCLUSIONS

Several classes of molecules undergo irreversible color and structural changes upon exposure to UV light, with well-defined mechanisms depending on the molecular structure, substituents, and experimental conditions. The BMT group of molecules distinguishes itself through its versatility and responsiveness to changes in structure, environment, and excitation energy, making them promising candidates for

applications requiring tailored optical properties. A unique property of BMT molecules is their ability to respond distinguishably to different parts of the UV spectrum, which could be exploited in sensing and monitoring applications, especially since the transformation process is irreversible. Our findings elucidate the factors governing the photocyclization behavior of these molecules and emphasize the importance of the molecular environment in controlling their photophysical properties. This understanding can guide the design and development of novel photochromic systems with tailored properties for applications, such as optical switches, sensors, and data storage devices. Further, beyond solution-based samples, these molecules can be incorporated into thin films, enabling the control and stabilization of emission properties in solid form. This opens possibilities for practical implementation in various fields, where tailored optical properties can be harnessed in a robust and scalable manner. The ease of fabrication and compatibility with flexible substrates make these thin films potential candidates for a wide range of optoelectronic and display applications such as large-area, flexible, and energy-efficient lighting solutions, gain medium in organic lasers, and luminescent solar concentrators with roll-to-roll processing capability. Finally, we demonstrate the possibility of a polymer-gel platform that has realistic potential of being developed into an active UV sensor.^{31,41,42}

EXPERIMENTAL SECTION

General Considerations. Caution. All procedures involving ultraviolet and laser radiations were conducted in accordance with institutional risk assessments. The 280 nm (21 mW, 1 mW/mm²) and 365 nm (120 mW, 6 mW/mm²) UV lamps, as well as the NKT Photonics Super-K laser at 430 nm, are categorized as sources of nonionizing radiation hazardous to biological tissue and eyesight. Experiments were performed in restricted-access areas with interlocked enclosures, and UV-specific signage was displayed throughout the workspace. All personnel wore UV-rated protective eyewear, lab coats, and nitrile gloves. Laser operation followed Class 3B safety protocols, including use of an emission indicator and interlock system. Risk assessment and photobiological safety limits (IEC 62471) were reviewed prior to experimentation.

Reagents and solvents were purchased at the highest commercial quality and used without purifications unless otherwise specified. Yields refer to chromatographically and spectroscopically (¹H NMR, ¹³C NMR) homogeneous material, unless otherwise noted. The yields in the publication and Supporting Information are the result of a single reaction. All reactions were carried out at room temperature. NMR spectra were recorded on a Varian-INOVA 400 or 500 MHz spectrometer and calibrated using residual undeuterated solvent as an internal reference (CDCl₃ – ¹H NMR: 7.26 ppm, ¹³C NMR: 77.16 ppm). The following abbreviations were used to explain multiplicities (s – singlet, d – doublet, t – triplet, q – quartet, m – multiplet). HRMS data was collected on Thermo Fisher Scientific Exactive Plus Orbitrap Mass Spectrometer. All masses reported are in regard to Bromine-79. All synthesized substrates were prepared according to literature procedures, which are described below. Absorption spectra are taken with a PerkinElmer UV–vis spectrophotometer. For static spectroscopy, a Princeton Instruments SP2300i spectrometer is employed, which is coupled to a thermo-electrically cooled, deep depletion, low noise charge-coupled device (CCD) detector. The system offers a spectral resolution of 0.18 nm. Excitation is provided by a 280 nm (21 mW, 1 mW/mm²) and a 365 nm (120 mW, 6 mW/mm²) UV lamp and an NKT Photonics Super-K laser tuned to 430 nm in the case of time-resolved measurements. The collected signal is first dispersed by the spectrometer and then directed onto a single photon avalanche diode (SPAD). The SPAD is coupled to a PicoHarp 300 time-correlated single photon counting (TCSPC) system, which has an instrument response function of 28 ps. Single-crystal X-ray

diffraction of H-BMT and H-PIMT was obtained from slow evaporation of acetonitrile/hexane (1:1) solution at 0 °C, and the X-ray diffraction (XRD) was obtained from a XtaLab Synergy by Rigaku Oxford D diffractometer using Mo K α radiation ($\lambda = 0.71073$ Å) with $\omega/2\theta$ scan mode at the temperature of 298 K. The single-crystal X-ray structures of H-BMT and H-PIMT were analyzed using Olex2 software. Crystallographic data for H-BMT

General Procedure (A) for Synthesis of Phenylglyoxal Hydrate. Procedure A was followed according to the previously published literature.³¹ Selenium(IV) dioxide (0.231 g, 2.1 mmol, 1.1 equiv) is added to the reaction vessel along with a stir bar, water (0.108 mL, 6.0 mmol, 3.3 equiv), and 4 mL of dioxane. It is then heated to 60 °C until all of the selenium(IV) dioxide has dissolved. Substituted acetophenone (2.0 mmol, 1.0 equiv) is added through septa via a syringe. The temperature is then increased to 101 °C and refluxed for 24 h. After 24 h, the reaction is removed from the hot plate and the conversion is checked via TLC. Once the reaction flask has cooled to room temperature, the solution is vacuum filtered through a pad of Celite to remove selenium. The filtrate is transferred to a clean reaction flask and concentrated in vacuo, and 10 mL of water is added to the solution. The reaction is heated to 101 °C under reflux, overnight. The reaction flask is removed from the hot plate and filtered while hot via a Buchner funnel to remove any excess selenium. The filtrate is allowed to cool to room temperature, and the precipitated solid is filtered via Buchner funnel and allowed to dry for an hour before being collected, which was used without further purification.

General Procedure (B) for Synthesis of Benzoyl Pyrazine (BP). The following dry reagents are added to the reaction flask along with a stir bar: substituted phenylglyoxal hydrate (3 mmol, 1.4 equiv), pyrazine (2.14 mmol, 1.0 equiv), ammonium persulfate (3 mmol, 1.4 equiv), and silver nitrate (0.24 mmol, 0.08 equiv). A mixture (50 mL) of 1:1 H₂O/DCM is added to the reaction flask followed by sulfuric acid (2.14 mmol, 1.0 equiv). The reaction flask is then heated to 40 °C for 24 h. The flask is removed from the hot plate, cooled to room temperature, and quenched with 25 mL of 4 M NaOH. The reaction is extracted 3 times with 25 mL of dichloromethane, and the combined organic extract is dried over magnesium sulfate and concentrated in vacuo. The crude material is purified via column chromatography with silica gel and a 20:80 ethyl acetate/hexane mixture, producing the final benzoyl pyrazine product.

General Procedure (C) for Synthesis of Methylated Benzoyl Pyrazinium (BMT). Benzoyl pyrazines (0.05 mmol, 1 equiv) are methylated using trimethyloxonium tetrafluoroborate (8.1 mg, 0.055 mmol, 1.1 equiv) in 0.5 mL of DCM heated at 40 °C overnight. The crude mixture is cooled to room temperature, and the solid precipitate is filtered out to give pure methylated benzoyl pyrazine (BMT).

General Procedure (D) for Synthesis of 10-Hydroxy-2-methylpyrazino[1,2-a]indol-2-ium Tetrafluoroborate (PIMT). Methylated benzoyl pyrazinium (BMT) was dissolved in acetonitrile to produce a 10 mM solution, which was then irradiated using a Thor Lab 280 nm UV light at 80 mW. Production of the product was monitored using ¹H NMR conversion every 30 min until full conversion (conversion >99%).

General Procedure for Preparing Thin Films. Samples for solution state analysis in PVA were prepared by adding a mixture of BMTs in acetonitrile to aqueous PVA. 1 mL of ACN was added to 286.1 mg of H-BMT to make 10 mM solution of BMT in ACN. Aqueous PVA solution was prepared by dissolving 300 mg of 99+% hydrolyzed PVA (Sigma-Aldrich) in 10 mL of deionized water under continuous stirring at 150 °C until the solution became transparent. The 2 and 0.25 mM BMT/PVA solutions were made by adding 400 μ L and 50 μ L, respectively, of the prepared BMT/ACN solution to 2 mL of the cooled down PVA aqueous solution under continuous stirring. Thin films of BMT/PIMT in a PVA matrix were made by drop casting 400 μ L of the prepared mixture on to glass slides left to dry overnight.

Phenyl(pyrazin-2-yl)methanone (H-BP). General procedure B was employed using 456 mg (3 mmol) of phenylglyoxal hydrate. The crude material is purified via column chromatography with silica gel

and a 20:80 ethyl acetate/hexane mixture, which afforded **H-BP** (130 mg, 33% yield). Yellow solid. $^1\text{H NMR}$ (500 MHz, CDCl_3) δ 9.25 (s, 1H), 8.78 (d, J = 2.6 Hz, 1H), 8.69 (s, 1H), 8.08 (d, J = 7.7 Hz, 2H), 7.64 (t, J = 7.4 Hz, 1H), 7.51 (t, J = 7.7 Hz, 2H). $^{13}\text{C}\{^1\text{H}\}$ NMR (126 MHz, CDCl_3) δ : 192.2, 149.9, 146.7, 146.1, 142.9, 135.5, 133.6, 130.9, 130.1, 128.4, 128.4. HRMS (ESI- TOF) m/z calcd. for $\text{C}_{11}\text{H}_8\text{N}_2\text{O}$ ($\text{M} + \text{H}$) $^+$ 185.0709, found 185.0706.

(4-Bromophenyl)(pyrazin-2-yl)methanone (Br-BP). General procedure B was employed using 693 mg (3 mmol) of 4-bromophenylglyoxal hydrate. The crude material is purified via column chromatography with silica gel and a 20:80 ethyl acetate/hexane mixture, which afforded **Br-BP** (107 mg, 19% yield). Beige solid. $^1\text{H NMR}$ (500 MHz, CDCl_3) δ 9.28 (s, 1H), 8.80 (d, J = 2.4 Hz, 1H), 8.69 (s, 1H), 8.01 (d, J = 8.2 Hz, 2H), 7.66 (d, J = 8.2 Hz, 2H). $^{13}\text{C}\{^1\text{H}\}$ NMR (126 MHz, CDCl_3) δ : 191.0, 149.4, 147.0, 146.2, 142.8, 134.2, 132.4, 131.7, 129.0. HRMS (ESI- TOF) m/z calcd. for $\text{C}_{11}\text{H}_7\text{BrN}_2\text{O}$ ($\text{M} + \text{H}$) $^+$ + 262.9815, found 262.9810.

Pyrazin-2-yl(*p*-tolyl)methanone (CH_3 -BP). General procedure B was employed using 498 mg (3 mmol) of 4-methylphenylglyoxal hydrate. The crude material is purified via column chromatography with silica gel and a 20:80 ethyl acetate/hexane mixture, which afforded **CH_3 -BP** (60 mg, 14% yield). Yellow solid. $^1\text{H NMR}$ (500 MHz, CDCl_3) δ 9.24 (d, J = 1.5 Hz, 1H), 8.78 (d, J = 2.5 Hz, 1H), 8.69 (dd, J = 2.5, 1.5 Hz, 1H), 8.00 (d, J = 8.0 Hz, 2H), 7.32 (d, J = 8.0 Hz, 2H), 2.46 (s, 3H). $^{13}\text{C}\{^1\text{H}\}$ NMR (126 MHz, CDCl_3) δ : 191.9, 150.3, 146.6, 146.0, 144.6, 142.9, 132.9, 131.0, 129.1, 29.9. HRMS (ESI- TOF) m/z calcd. for $\text{C}_{12}\text{H}_{10}\text{N}_2\text{O}$ ($\text{M} + \text{H}$) $^+$ + 199.0866, found 199.0863.

4-(Pyrazine-2-carbonyl)benzotrile (CN-BP). General procedure B was employed using 531 mg (3 mmol) of 4-cyanophenylglyoxal hydrate. The crude material is purified via column chromatography with silica gel and a 20:80 ethyl acetate/hexane mixture, which afforded **CN-BP** (99 mg, 22% yield). Yellow solid. $^1\text{H NMR}$ (500 MHz, CDCl_3) δ : 9.34 (s, 1H), 8.84 (d, J = 2.2 Hz, 1H), 8.69 (s, 1H), 8.22 (d, J = 8.2 Hz, 2H), 7.81 (d, J = 8.2 Hz, 2H). ^{13}C NMR (126 MHz, CDCl_3) δ : 190.9, 148.7, 147.7, 146.5, 143.1, 139.0, 132.2, 131.4, 118.1, 116.7. HRMS (ESI- TOF) m/z calcd. for $\text{C}_{12}\text{H}_7\text{N}_3\text{O}$ ($\text{M} + \text{H}$) $^+$ + 210.0662, found 210.0656.

Phenyl(quinoxalin-2-yl)methanone (Quin-BP). General procedure B was employed using 456 mg of phenylglyoxal hydrate. The crude material is purified via column chromatography with silica gel and a 20:80 ethyl acetate/hexane mixture, which afforded **Quin-BP** (232 mg, 46% yield). Beige solid. $^1\text{H NMR}$ (500 MHz, CDCl_3) δ 9.48 (s, 1H), 8.24 – 8.19 (m, 4H), 7.93 – 7.82 (m, 2H), 7.65 (dd, J = 7.5 Hz, 1H), 7.53 (dd, J = 8.0 Hz, 2H). $^{13}\text{C}\{^1\text{H}\}$ NMR (126 MHz, CDCl_3) 192.4, 148.7, 145.4, 143.2, 140.5, 135.6, 133.7, 132.1, 131.3, 130.9, 130.5, 130.0, 129.5, 128.5, 127.5. HRMS (ESI- TOF) m/z calcd. for $\text{C}_{15}\text{H}_{10}\text{N}_2\text{O}$ ($\text{M} + \text{H}$) $^+$ + 235.0866, found 235.0861.

3-Benzoyl-1-methylpyrazin-1-ium Tetrafluoroborate (H-BMT). General procedure C was employed using 9.2 mg of **H-BP** and afforded **H-BMT** (13.2 mg, 92% yield). Green solid. $^1\text{H NMR}$ (500 MHz, CD_3CN) δ 9.45 (s, 1H), 9.32 (s, 1H), 8.99 (s, 1H), 8.07 (d, J = 7.74, 2H), 7.77 (t, J = 7.36, 1H), 7.60 (t, J = 7.64, 2H), 4.48 (s, 3H). $^{13}\text{C}\{^1\text{H}\}$ NMR (126 MHz, CD_3CN) δ : 188.8, 155.0, 149.2, 139.3 (t), 138.9 (t), 134.7, 134.0, 131.0, 128.7, 49.7. HRMS (ESI- TOF) m/z calcd. for $\text{C}_{12}\text{H}_{11}\text{N}_2\text{O}^+$ (M^+) 199.0866, found 199.0865.

3-(4-Bromobenzoyl)-1-methylpyrazin-1-ium Tetrafluoroborate (Br-BMT). General procedure C was employed using 13.1 mg of **Br-BP** and afforded **Br-BMT** (12.1 mg, 66% yield). Green solid. $^1\text{H NMR}$ (500 MHz, CD_3CN) δ 9.48 (d, J = 2.9 Hz, 1H), 9.29 (s, 1H), 8.89 (d, J = 3.6 Hz, 1H), 8.09 – 7.96 (m, 2H), 7.90 – 7.76 (m, 2H), 4.51 (s, 3H). $^{13}\text{C}\{^1\text{H}\}$ NMR (126 MHz, CD_3CN) δ 188.5, 155.7, 150.4, 140.3 (t), 140.2 (t), 133.9, 133.6, 133.0, 130.6, 50.6 (t). HRMS (ESI- TOF) m/z calcd. for $\text{C}_{12}\text{H}_{10}\text{BrN}_2\text{O}^+$ (M^+) 276.9971, found 276.9969.

1-Methyl-3-(4-methylbenzoyl)pyrazin-1-ium Tetrafluoroborate (CH_3 -BMT). General procedure C was employed using 9.9 mg of **CH_3 -BP** and afforded **CH_3 -BMT** (6 mg, 57% yield). Green solid. $^1\text{H NMR}$ (500 MHz, CD_3CN) δ 9.47 (q, J = 3.1 Hz, 1H), 9.24 (s, 1H), 8.87 (d, J = 3.4 Hz, 1H), 8.08 – 7.97 (m, 2H), 7.46 (d, J = 8.0 Hz,

2H), 4.50 (s, 3H), 2.50 (s, 3H). $^{13}\text{C}\{^1\text{H}\}$ NMR (126 MHz, CD_3CN) δ 188.9, 156.6, 150.4, 147.5, 140.0 (t), 132.1, 130.4, 50.5 (t), 21.9. HRMS (ESI- TOF) m/z calcd. for $\text{C}_{13}\text{H}_{13}\text{N}_2\text{O}^+$ (M^+) 213.1022, found 213.1019.

3-(4-Cyanobenzoyl)-1-methylpyrazin-1-ium Tetrafluoroborate (CN-BMT). General procedure C was employed using 10.4 mg of **CN-BP** and afforded **CN-BMT** (13.2 mg, 85% yield). Green solid. $^1\text{H NMR}$ (500 MHz, CD_3CN) δ 9.45 (s, 1H), 9.30 (s, 1H), 8.90 (d, J = 3.1 Hz, 1H), 8.18 (d, J = 8.2 Hz, 2H), 7.95 (d, J = 8.3 Hz, 2H), 4.50 (s, 3H). $^{13}\text{C}\{^1\text{H}\}$ NMR (126 MHz, CD_3CN) δ 188.7, 155.0, 150.5, 140.7, 140.6 (t), 140.45 (t), 138.2, 133.5, 132.3, 118.8, 118.1, 50.7 (t) HRMS (ESI- TOF) m/z calcd. for $\text{C}_{13}\text{H}_{10}\text{N}_3\text{O}^+$ (M^+) 224.0818, found 224.0811.

3-Benzoyl-1-methylquinoxalin-1-ium Tetrafluoroborate (Quin-BMT). General procedure C was employed using 11.7 mg of **Quin-BP** and afforded **Quin-BMT** (16.1 mg, 96% yield). Orange solid. $^1\text{H NMR}$ (500 MHz, CD_3CN) δ 9.66 (s, 1H), 8.61 – 8.52 (m, 2H), 8.46 (dd, J = 8.0 Hz, 1H), 8.40 – 8.34 (m, 1H), 8.23 (d, J = 8.0 Hz, 2H), 7.80 (dd, J = 7.5 Hz, 1H), 7.64 (dd, J = 7.5 Hz, 2H), 4.79 (s, 3H). ^{13}C NMR (126 MHz, CD_3CN) δ : 189.2, 156.6, 150.6, 140.2 (t), 140.0 (t), 137.0, 135.5, 133.1, 132.3, 130.9, 130.8, 129.7, 128.9, 128.5, 125.9, 50.6 (t). HRMS (ESI- TOF) m/z calcd. for $\text{C}_{16}\text{H}_{13}\text{N}_2\text{O}^+$ (M^+) 249.1022, found 249.1017.

10-Hydroxy-2-methylpyrazino[1,2-*a*]indol-2-ium Tetrafluoroborate (H-PIMT). General procedure D was employed using 2.86 mg (10 mM) of **H-BMT** for 1.5 h and afforded **H-PIMT** (2.86 mg, > 99% yield). Red solid. $^1\text{H NMR}$ (500 MHz, CD_3CN) δ 8.98 (s, 1H), 8.41 (d, J = 5.0 Hz, 1H), 8.10 (d, J = 10.0 Hz, 1H), 8.05 (d, J = 5.0 Hz, 1H), 7.73 (dd, J = 10 Hz, 1H), 7.54 (dd, J = 10 Hz, 1H), 6.92 (dd, J = 5.9, 1.4 Hz, 1H), 3.97 (s, 3H). $^{13}\text{C}\{^1\text{H}\}$ NMR (126 MHz, CD_3CN) δ : 144.32, 142.32, 131.51, 129.90, 125.2, 122.1, 121.5, 119.6, 115.2, 115.0, 113.3, 47.0. HRMS (ESI- TOF) m/z calcd. for $\text{C}_{12}\text{H}_{11}\text{N}_2\text{O}^+$ (M^+) 199.0866, found 199.0862.

7-Bromo-10-hydroxy-2-methylpyrazino[1,2-*a*]indol-2-ium Tetrafluoroborate (Br-PIMT). General procedure D was employed using 3.64 mg (10 mM) of **Br-BMT** for 3.5 h and afforded **Br-PIMT** (3.64 mg, > 99% yield). Red solid. $^1\text{H NMR}$ (500 MHz, CD_3CN) δ 8.99 (s, 1H), 8.86 (s, 1H), 8.35 (s, 1H), 8.01 (d, J = 9.0 Hz, 1H), 7.63 (dd, J = 9.0, 1.5 Hz, 1H), 6.94 (dd, J = 6.0, 1.4 Hz, 1H), 3.96 (s, 3H). $^{13}\text{C}\{^1\text{H}\}$ NMR (126 MHz, CD_3CN) δ : 144.85, 142.31, 133.02, 131.54, 128.59, 123.37, 123.19, 122.10, 116.53, 116.03, 115.37, 47.16. HRMS (ESI- TOF) m/z calcd. for $\text{C}_{12}\text{H}_{10}\text{BrN}_2\text{O}^+$ (M^+) 276.9971, found 276.9966.

10-Hydroxy-2,7-dimethylpyrazino[1,2-*a*]indol-2-ium Tetrafluoroborate (CH_3 -PIMT). General procedure D was employed using 3.00 mg (10 mM) of **CH_3 -BMT** for 4 h and afforded **CH_3 -PIMT** (3.00 mg, > 99% yield). Red solid. $^1\text{H NMR}$ (500 MHz, CD_3CN) δ 8.90 (s, 1H), 8.72 (s, 1H), 8.30 (d, J = 6.0 Hz, 1H), 7.98 (d, J = 8.5 Hz, 1H), 7.84 (d, J = 0.5 Hz, 1H), 7.39 (d, J = 9.0 Hz, 1H), 6.86 (dd, J = 6.0, 1.5 Hz, 1H), 3.93 (s, 3H), 2.60 (s, 3H). $^{13}\text{C}\{^1\text{H}\}$ NMR (126 MHz, CD_3CN) δ : 143.9, 142.3, 141.5, 132.1, 130.4, 127.8, 121.5, 121.2, 115.3, 114.9, 112.1, 46.8, 22.6. HRMS (ESI- TOF) m/z calcd. for $\text{C}_{13}\text{H}_{13}\text{N}_2\text{O}^+$ (M^+) 213.1022, found 213.1020.

7-Cyano-10-hydroxy-2-methylpyrazino[1,2-*a*]indol-2-ium Tetrafluoroborate (CN-PIMT). General procedure D was employed using 3.11 mg (10 mM) of **CN-BMT** for 1.5 h and afforded **CN-PIMT** (3.11 mg, > 99% yield). Red solid. $^1\text{H NMR}$ (500 MHz, CD_3CN) δ 9.12 (s, 2H), 8.59 (s, 2H), 8.50 (d, J = 5.9 Hz, 2H), 8.23 (d, J = 8.7 Hz, 2H), 7.71 (d, J = 8.8 Hz, 2H), 7.07 (d, J = 5.8 Hz, 2H), 4.04 (s, 3H). $^{13}\text{C}\{^1\text{H}\}$ NMR (126 MHz, CD_3CN) δ . 144.4, 140.8, 140.3, 132.6, 131.3, 126.5, 125.0, 122.1, 122.0, 119.9, 119.0, 118.60, 115.7, 46.7. HRMS (ESI- TOF) m/z calcd. for $\text{C}_{13}\text{H}_{10}\text{N}_3\text{O}^+$ (M^+) 224.0818, found 224.0816.

7-Hydroxy-5-methylindolo[1,2-*a*]quinoxalin-5-ium Tetrafluoroborate (Quin-PIMT). General procedure D was employed using 3.36 mg (10 mM) of **Quin-BMT** for 4 h and afforded **Quin-PIMT** (3.36 mg, > 99% yield). Red solid. $^1\text{H NMR}$ (500 MHz, CD_3CN) δ 9.08 (s, 1H), 8.49 (dd, J = 20.0 Hz, 2H), 8.22 (d, J = 10.0 Hz, 1H), 7.91 – 7.88 (m, 2H), 7.81 (t, J = 15.0 Hz, 1H), 7.57 (q, J = 15.0 Hz, 2H), 4.13 (s, 3H). $^{13}\text{C}\{^1\text{H}\}$ NMR (126 MHz, CD_3CN) δ :

148.6, 145.9, 135.6, 132.8, 132.3, 131.7, 127.2, 126.1, 124.2, 122.9, 120.8, 119.7, 117.5, 115.7, 115.3, 44.5. HRMS (ESI) m/z calcd. for $C_{16}H_{13}N_2O^+$ (M^+) 249.1022, found 249.1017.

■ ASSOCIATED CONTENT

Data Availability Statement

The data underlying this study are available in the published article and its [Supporting Information](#).

Supporting Information

The Supporting Information is available free of charge at <https://pubs.acs.org/doi/10.1021/acs.joc.5c01311>.

Spectroscopic data for all relevant materials ([PDF](#))

■ AUTHOR INFORMATION

Corresponding Authors

Sayantani Ghosh – Department of Physics, University of California, California 95343, United States; orcid.org/0000-0003-3440-7194; Email: sghosh@ucmerced.edu

Ryan D. Baxter – Department of Chemistry and Biochemistry, University of California, California 95343, United States; orcid.org/0000-0002-1341-5315; Email: rbaxter@ucmerced.edu

Authors

Arya K. Rajan – Department of Physics, University of California, California 95343, United States

Pravien S. Rajaram – Department of Chemistry and Biochemistry, University of California, California 95343, United States

Keerthana Chakkanalil – Department of Chemistry and Biochemistry, University of California, California 95343, United States

Complete contact information is available at:

<https://pubs.acs.org/doi/10.1021/acs.joc.5c01311>

Author Contributions

[‡]A.K.R. and P.S.R. contributed equally. The manuscript was written through contributions of all authors. All authors have given approval to the final version of the manuscript.

Notes

The authors declare no competing financial interest.

■ ACKNOWLEDGMENTS

The authors acknowledge funding from the National Science Foundation awards no. DGE-2125510 and HRD-2112675. The authors thank Mourad Sadqi and the Mass Spectrometry Unit of the Center for Cellular and Biomolecular Machines (CCBM) NSF-CREST program for their assistance with mass spectrometry data analysis and processing.

■ REFERENCES

- (1) Tang, C. W.; VanSlyke, S. A. Organic electroluminescent diodes. *Appl. Phys. Lett.* **1987**, *51* (12), 913–915.
- (2) Yin, X.; He, Y.; Wang, X.; Wu, Z.; Pang, E.; Xu, J.; Wang, J.-A. Recent advances in thermally activated delayed fluorescent polymer-molecular designing strategies. *Front. Chem.* **2020**, *8*, 725.
- (3) Reineke, S.; Lindner, F.; Schwartz, G.; Seidler, N.; Walzer, K.; Lussem, B.; Leo, K. White organic light-emitting diodes with fluorescent tube efficiency. *Nature* **2009**, *459* (7244), 234–238.
- (4) Wu, J.-Y.; Chen, S.-A. Development of a highly efficient hybrid white organic-light-emitting diode with a single emission layer by solution processing. *ACS Appl. Mater. Interfaces* **2018**, *10* (5), 4851–4859.

(5) Lavis, L. D.; Raines, R. T. Bright building blocks for chemical biology. *ACS Chem. Biol.* **2014**, *9* (4), 855–866.

(6) Ma, J.; Shu, T.; Sun, Y.; Zhou, X.; Ren, C.; Su, L.; Zhang, X. Luminescent covalent organic frameworks for biosensing and bioimaging applications. *Small* **2022**, *18* (3), No. 2103516.

(7) Zhang, J. F.; Zhou, Y.; Yoon, J.; Kim, J. S. Recent progress in fluorescent and colorimetric chemosensors for detection of precious metal ions (silver, gold and platinum ions). *Chem. Soc. Rev.* **2011**, *40* (7), 3416–3429.

(8) Zielonka, J.; Kalyanaraman, B. Small-molecule luminescent probes for the detection of cellular oxidizing and nitrating species. *Free Radical Biol. Med.* **2018**, *128*, 3–22.

(9) Luo, D.; Jang, W.; Babu, D. D.; Kim, M. S.; Wang, D. H.; Kyaw, A. K. K. Recent progress in organic solar cells based on non-fullerene acceptors: materials to devices. *Journal of Materials Chemistry A* **2022**, *10* (7), 3255–3295.

(10) Guo, J.; Zhen, Y.; Dong, H.; Hu, W. Recent progress on organic exciplex materials with different donor–acceptor contacting modes for luminescent applications. *Journal of Materials Chemistry C* **2021**, *9* (47), 16843–16858.

(11) Scholz, S.; Kondakov, D.; Lussem, B.; Leo, K. Degradation mechanisms and reactions in organic light-emitting devices. *Chem. Rev.* **2015**, *115* (16), 8449–8503.

(12) Zhang, J.; Han, M.; Xu, M.; Zhang, L.; Liu, S.; Xie, W. Color-tunable organic light-emitting devices and their applications. *Cell Reports Physical Science* **2024**, *5* (1), No. 101764.

(13) Wen, H.-M.; Wu, Y.-H.; Xu, L.-J.; Zhang, L.-Y.; Chen, C.-N.; Chen, Z.-N. Luminescent square-planar platinum (ii) complexes with tridentate 3-bis (2-pyridylimino) isoindoline and monodentate n-heterocyclic ligands. *Dalton Transactions* **2011**, *40* (26), 6929–6938.

(14) Mei, J.; Leung, N. L.; Kwok, R. T.; Lam, J. W.; Tang, B. Z. Aggregation-induced emission: together we shine, united we soar! *Chem. Rev.* **2015**, *115* (21), 11718–11940.

(15) Yin, C.; Yan, Z.-A.; Ma, X. Supramolecular assembly strategy towards organic luminescent materials. *Chem. Commun.* **2023**, *59*, 13421–13433.

(16) Chen, C.-T. Evolution of red organic light-emitting diodes: materials and devices. *Chem. Mater.* **2004**, *16* (23), 4389–4400.

(17) Zhu, C.; Kwok, R. T.; Lam, J. W.; Tang, B. Z. Aggregation-induced emission: a trailblazing journey to the field of biomedicine. *ACS Applied Biomaterials* **2018**, *1* (6), 1768–1786.

(18) Mukherjee, S.; Thilagar, P. Recent advances in purely organic phosphorescent materials. *Chem. Commun.* **2015**, *51* (55), 10988–11003.

(19) Zhao, J.; Xu, K.; Yang, W.; Wang, Z.; Zhong, F. The triplet excited state of BODIPY: formation, modulation and application. *Chem. Soc. Rev.* **2015**, *44* (24), 8904–8939.

(20) Wong, M. Y.; Zysman-Colman, E. Purely organic thermally activated delayed fluorescence materials for organic light-emitting diodes. *Adv. Mater.* **2017**, *29* (22), No. 1605444.

(21) Yuan, L.; Lin, W.; Zheng, K.; He, L.; Huang, W. Far-red to near infrared analyte-responsive fluorescent probes based on organic fluorophore platforms for fluorescence imaging. *Chem. Soc. Rev.* **2013**, *42* (2), 622–661.

(22) Li, F.; Wang, M.; Liu, S.; Zhao, Q. Halide-containing organic persistent luminescent materials for environmental sensing applications. *Chemical Science* **2022**, *13* (8), 2184–2201.

(23) Cavinato, L. M.; Yamaoka, K.; Lipinski, S.; Calvi, V.; Wehenkel, D.; van Rijn, R.; Albrecht, K.; Costa, R. D. Dendri-LEC family: Establishing the bright future for dendrimer emitters in traditional and graphene-based light-emitting electrochemical cells. *Adv. Funct. Mater.* **2023**, *33* (35), No. 2302483.

(24) Ren, M.; Cao, S.; Zhao, J.; Zou, B.; Zeng, R. Advances and challenges in two-dimensional organic–inorganic hybrid perovskites toward high-performance light-emitting diodes. *Nano-Micro Lett.* **2021**, *13*, 163.

(25) Cui, L.-S.; Nomura, H.; Geng, Y.; Kim, J. U.; Nakanotani, H.; Adachi, C. Controlling singlet–triplet energy splitting for deep-blue

thermally activated delayed fluorescence emitters. *Angew. Chem., Int. Ed.* **2017**, *56* (6), 1571–1575.

(26) Jiang, H.; Zhang, L.; Xian, L.; Wang, Z.; Jin, J.; Zheng, C.; Chen, R. AIE-active organic resonance molecules for highly sensitive dynamic explosive detection. *Journal of Materials Chemistry C* **2022**, *10* (21), 8241–8245.

(27) Hurt, C. R.; Filipescu, N. Photocyclization of Di(2-pyridyl) Ketone and 2-Benzoylpyridine in Aqueous Solution. *J. Am. Chem. Soc.* **1972**, *94*, 3649–3651.

(28) Elisei, F.; Favaro, G.; Romani, A. A Laser Flash Photolysis Study of Di-Pyridyl Ketones. *Chem. Phys.* **1990**, *144*, 107–115.

(29) Atfah, A.; Abu-Shuheil, M. Y.; Hill, J. Photocyclisation of 2-Aroylquinoxalines; Formation of Coloured Indolo[1,2-a]-Quinoxalines. *Tetrahedron* **1990**, *46* (18), 6483–6500.

(30) Du, Y.; Xue, J.; Li, M.-D.; Guan, X.; McCamant, D. W.; Phillips, D. L. Unravelling the Reaction Mechanism for the Fast Photocyclisation of 2-Benzoylpyridine in Aqueous Solvent by Time-Resolved Spectroscopy and Density Functional Theory Calculations, *Chemistry. European Journal* **2010**, *16*, 6961–6972.

(31) Brisbin, R. P.; Rajan, A. K.; Khan, M. I.; Rajaram, P. S.; Russell, K. M.; Ghosh, S.; Baxter, R. D. Concentration-dependent emission from low molecular weight benzoyl pyrazinium salts. *Materials Advances* **2023**, *4* (23), 6271–6276.

(32) Zade, S. S.; Zamoshchik, N.; Bendikov, M. From short conjugated oligomers to conjugated polymers. lessons from studies on long conjugated oligomers. *Acc. Chem. Res.* **2011**, *44* (1), 14–24.

(33) Yamana, K.; Kawasaki, R.; Sugikawa, K.; Ikeda, A. Solubilization of Tetrahydroxyphenylchlorin in Water and Improved Photodynamic Activity after Complexation with Cyclic Oligo- and Polysaccharides. *ACS Applied Bio Materials* **2020**, *3* (5), 3217–3225.

(34) Pogue, B. W.; Samkoe, K. S.; Gibbs-Strauss, S. L.; Davis, S. C. Fluorescent Molecular Imaging and Dosimetry Tools in Photodynamic Therapy. In *Photodynamic Therapy: Methods and Protocols*; Gomer, C. (eds), Methods in Molecular Biology, Humana Press: 2010, 207–222.

(35) Wang, X.; Hu, Y.-Z.; Chen, A.; Wu, Y.; Aggeler, R.; Low, Q.; Kang, H. C.; Gee, K. R. Water-soluble poly (2, 7-dibenzosilole) as an ultra-bright fluorescent label for antibody-based flow cytometry. *Chem. Commun.* **2016**, *52* (21), 4022–4024.

(36) Prorot, A.; Chazal, P.; Leprat, P. Flow cytometry as a powerful tool for monitoring microbial population dynamics in sludge. In *Flow Cytometry-Recent Perspectives*; IntechOpen: 2012.

(37) Iftikhar, R.; Parveen, I.; Ayesha; Mazhar, A.; Iqbal, M. S.; Kamal, G. M.; Hafeez, F.; Pang, A. Y.; Ahmadipour, M. Small organic molecules as fluorescent sensors for the detection of highly toxic heavy metal cations in portable water. *J. Environ. Chem. Eng.* **2023**, *11* (1), No. 109030.

(38) Klymchenko, A. S. Solvatochromic and fluorogenic dyes as environment-sensitive probes: design and biological applications. *Acc. Chem. Res.* **2017**, *50* (2), 366–375.

(39) Yang, Y.; Gao, F.; Wang, Y.; Li, H.; Zhang, J.; Sun, Z.; Jiang, Y. Fluorescent organic small molecule probes for bioimaging and detection applications. *Molecules* **2022**, *27* (23), 8421.

(40) Delmas, W. G.; Vickers, E. T.; DiBenedetto, A. C.; Lum, C.; Hernandez, I. N.; Zhang, J. Z.; Ghosh, S. Modulating charge carrier dynamics and transfer via surface modifications in organometallic halide perovskite quantum dots. *J. Phys. Chem. Lett.* **2020**, *11* (18), 7886–7892.

(41) This work is based on the following thesis defense: Rajaram, P.; Baxter, R. *Innovative Approaches For Nitrogen Incorporation Into Organic Small Molecules: Synthesis For Application*. UC Merced: 2025. ProQuest ID: Rajaram_ucmerced_1660D_11230. Merritt ID: ark:/13030/m5n992q1. Retrieved from <https://escholarship.org/uc/item/56q5j9kn>.

(42) This work is based on the following preliminary patent: Baxter, D. R.; Brisbin, R. P.; Ghosh, S. Luminescent Benzoyl-Pyrazine Organic Compounds. U. S. Patent Application No. US18/862,112, July 17, 2025.



CAS INSIGHTS™

EXPLORE THE INNOVATIONS
SHAPING TOMORROW

Discover the latest scientific research and trends with CAS Insights. Subscribe for email updates on new articles, reports, and webinars at the intersection of science and innovation.

Subscribe today

CAS
A Division of the
American Chemical Society